Performance evaluation of a coupled CFX-RELAP5 tool adopting experimental data from the TALL-3D facility

Nuclear Engineering and Design 432 (2025) 113818

Contents lists available at ScienceDirect

Nuclear Engineering and Design

journal homepage: www.elsevier.com/locate/nucengdes

Performance evaluation of a coupled CFX-RELAP5 tool adopting experimental data from the TALL-3D facility☆

P. Cioli Puviani [a,*], T. Del Moro [b], B. Gonfiotti [c], D. Martelli [c], C. Ciurluini [b], F. Giannetti [b], R. Zanino [a], M. Tarantino [c]

[a] NEMO Group, Dipartimento Energia, Politecnico di Torino, Corso Duca degli Abruzzi, 24, 10129 Torino, Italy
[b] Department of Astronautical, Electrical and Energy Engineering DIAEE, Sapienza University of Rome, Corso Vittorio Emanuele II, 244, 00186 Rome, Italy
[c] ENEA Brasimone, 40032 Camugnano, Bologna, Italy

ARTICLE INFO

Keywords:
CFD
STH
HLM
Coupling
TALL-3D

ABSTRACT

The interest for multiscale simulations for the thermal–hydraulic analysis of nuclear systems has increased with the grow of computational power and the need of complex three-dimensional analysis for the generation IV nuclear reactors. To perform analyses at different scales, coupling codes are expected to be a valuable solution. Particularly, the coupling between System Thermal Hydraulic (STH) and Computational Fluid Dynamics (CFD) codes promises to achieve the goal of a detailed local solution at CFD level, while keeping the speed of a STH approach elsewhere in the system, where 1D phenomena are predominant. The validation of new developed coupled tools requires specific experimental facilities in which three-dimensional phenomena affect the behaviour of the entire system. TALL-3D is a liquid Lead Bismuth Eutectic loop designed in such a way to produce experimental data for coupled STH and CFD codes validation. In this work, a Ansys CFX – RELAP5/Mod3.3 coupled tool is adopted to replicate a forced to natural circulation transition on the TALL-3D facility, comparing different coupling strategies regarding the spatial domain discretization (decomposition and overlapping) and time advancing scheme (explicit and semi-implicit). Results obtained with the coupled models show a clear advantage with respect to the RELAP5 standalone one. The analysis of the phenomena involved show the inability of the STH code in reproducing them, while the coupled tool proved to be a reliable solution thanks to its capability to take advantage of both the component and system scales analysis. Moreover, the impact of the selected coupling strategy on the stability of the tool is assessed, and the required computational time for the analysed transient is evaluated.

1. Introduction

In the nuclear field, the Thermal-Hydraulic (TH) analysis of the phenomena inside reactors drives the design and improvements of new systems and components (Frignani et al., 2019). Furthermore, it plays a fundamental role in reactor safety assessment by demonstrating the system's ability to reach safe conditions during off-normal and accidental scenarios.

Within Generation IV nuclear reactors, Lead-cooled Fast Reactors (LFRs) are considered among the most promising technologies. They offer several advantages, including efficient fuel utilization, inherent safety features, and the ability to transmute nuclear waste. The properties of the coolant make it possible to open up to a pool-type configuration, in which all the systems and components of the primary circuit are enclosed within the reactor vessel. Due to these innovative characteristics, unique challenges linked to the reactor's primary side need to be addressed (Lorusso et al., 2018).

System Thermal-Hydraulic (STH) – Computational Fluid Dynamics (CFD) coupling tools are gaining increasing interest to solve part of the thermal–hydraulic open issues (Toti, 2018). STH codes excel at modelling the overall TH behaviour of the reactor adopting a mono-dimensional representation of the components, running with limited computational time and providing reliable prediction with multiphase fluids. CFD excels at describing the fluid flow with a greater detail within the reactor components compared to the STH codes, with improved performance in domains where three-dimensional phenomena are

☆ This article is part of a special issue entitled: 'LFR' published in Nuclear Engineering and Design.

* Corresponding author.
E-mail address: pietro.ciolipuviani@polito.it (P. Cioli Puviani).

https://doi.org/10.1016/j.nucengdes.2024.113818
Received 7 October 2024; Received in revised form 2 December 2024; Accepted 29 December 2024
Available online 31 December 2024

relevant, although, at the cost of a computational burden (Gibeling and Mahaffy, 2002). By coupling these two approaches, it is possible to gain a broader understanding of the LFR TH phenomena at component scale, with a global representation of the system and a multi-scale approach that could lead to improved system simulation with acceptable computational time.

Nonetheless, the adoption of new tools brings the necessity of validation against high quality experimental data. The coupled tools validation could be carried out on small scale known problem, as pipe T-junction (Bertolotto et al., 2009), or loop facilities with components that exhibit reproducible behaviour with one-dimensional approximations: with these cases is possible to prove the consistency and robustness of the coupling strategy and no-to-little discrepancies with STH code are foreseen (Martelli et al., 2014). An example of loop type facility is the NACIE-UP facility (Del Moro et al., 2024), a LBE loop where transition from forced to natural circulation has been tested: if the phenomena inside components could be represented by well-known correlations for what concern the heat transfer and the pressure drops, in those case the CFD – STH, should not provide, in general, improved results at the system level with respect to the STH standalone code. However, the additional information provided by the CFD code consist in a three-dimensional insight within specific components, such as the Fuel Pin Bundle Simulator, giving the possibility to deepening the phenomenological analysis.

To test coupled CFD-STH tools, experimental tests in which STH codes are expected to fail should be designed. The limitations of STH have been discussed in the THINS European project and reported in Bandini et al. (2015), where it is highlighted that CFD is crucial to reproduce phenomena such as stratification, solidification, thermal mixing and cases where three-dimensional solid and fluid conduction plays a fundamental role. A particular scenario in which STH codes could fail is in the prediction of passive safety systems behaviour in pool type reactors: the interaction between pool thermal dynamics and the forces that drive natural circulation can create complex transient phenomena, occurring at different spatial and time scales (Moreau et al., 2019).

The TALL-3D facility, described in Section 2, has been designed with the purpose of evaluating the advantages of coupled tools and validating them against experimental results. Due to mutual feedback between natural circulation in the loop and complex 3D mixing and stratification phenomena in the axisymmetric pool-type test section, the facility consists in an optimal test case for the coupled tools validation, largely adopted in literature for this purpose (Papukchiev et al., 2015).

The performances of the standalone CFD model of the 3D test section (computed with CFX) are presented in Section 3 for steady state and transient conditions coming from a forced to natural circulation transition experiment.

The Ansys CFX – RELAP5/Mod3.3 coupled tool is then presented. An alternative overlapping domain method, which has been discussed in the literature for other codes (Huxford et al., 2023), is used. The results are discussed along with the overlapping method previously presented by the authors (Cioli Puviani et al., 2025) and with simulations that adopts a decomposition approach. Furthermore, the impact of different time advancing schemes, explicit and semi-implicit, is presented. Eventually the coupled tool results are compared with the STH ones and validated against the experimental results, both at component and system scale for the considered transient.

2. TALL-3D facility

The facility (Fig. 1) is mainly composed by the primary loop, with Lead-Bismuth Eutectic (LBE) as coolant, and the secondary loop, with the synthetic organic heat transfer fluid Dowtherm RP, for a facility's total height of 6.5 m.

The primary loop comprises the sump tank (on the left) for storing, melting, and supplying LBE to the main loop, three vertical legs, and two horizontal sections connecting each pair of elbows and a T-junction. The Main Heater (MH) leg (left leg) contains a 27 kW rod-type electric heater

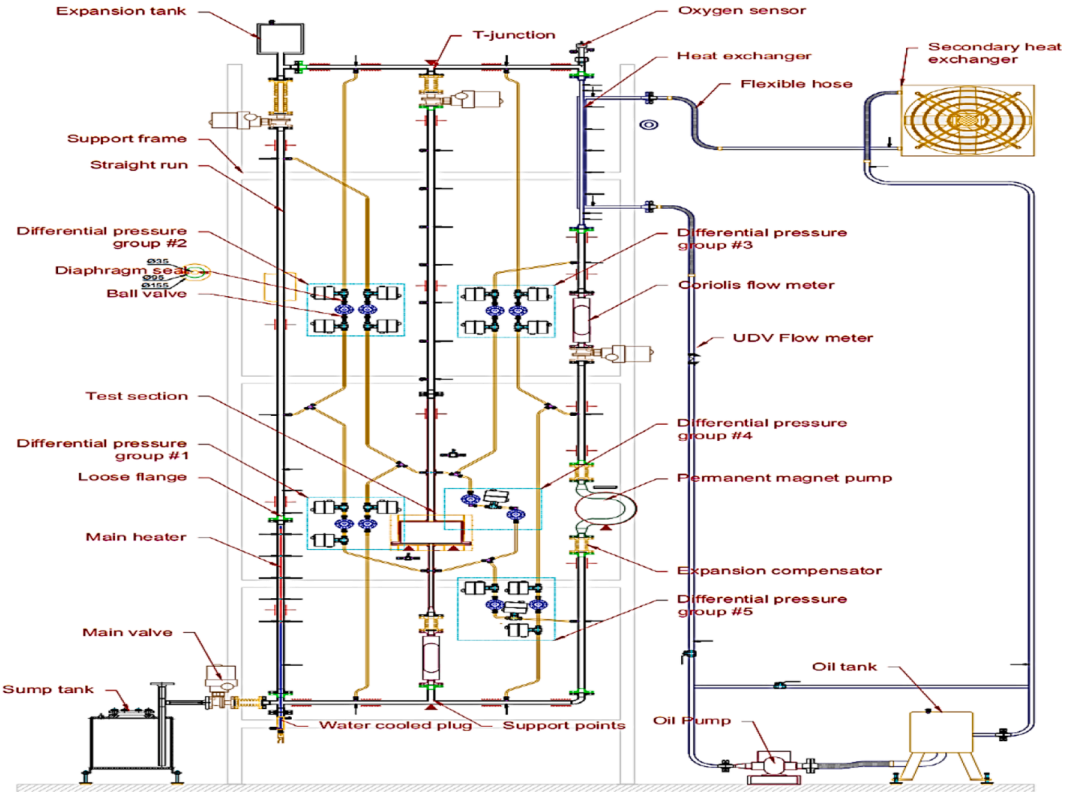

Fig. 1. TALL-3D facility main components (Grishchenko et al., 2015).

(pin outer diameter 8.2 mm, heated length 870 mm) at the bottom (Fig. 2a) and an expansion tank at the top. The Heat Exchanger (HX) leg (right leg) consists in a counter-current heat exchanger (Fig. 2b) at the top and an Electric Permanent Magnet (EPM) pump at the bottom (Fig. 2c). The middle 3D leg connects a pool-type 3D test section to the loop.

The 3D Test section (3D-TS) is an axisymmetric cylindrical stainless steel vessel with a bottom and a top connection to the loop (see Fig. 3a). The geometrical description and the instrumentation position could be found in Grishchenko et al. (2015). The upper two-thirds of the test section feature a 15 kW band heater around its circumference to promote thermal stratification in the LBE pool. Inside, a circular plate is mounted perpendicular to the flow path to enhance pool mixing by deflecting the flow entering from the bottom toward the periphery. The plate is attached to the pool ceiling with four fin-shaped separators, designed to minimize flow disturbance. The 3D-TS inlet tube has a lower diameter than the outlet one (inner/outer diameter of 17/23 mm instead of 27.8/33.4 mm). The latter has the same dimension of the pipes connecting the primary loop's main components.

Two types of thermal insulators are used: ISOVER Tape Lock 7300 and Nano T Ultra. Nano T Ultra is used only for some regions around the test section, ISOVER Tape Lock 7300 is used in the rest of the loop.

In Fig. 3b, the thermocouples (TCs) inside the 3D-TS are reported for a generic plane, indicated by the "x" letter, of the four measuring planes present. For the validation of the pool modelling an ordinated vector has been built, only considering the instruments in the fluid, with the following order: CIP, BP, IPT, ILW (for the acronyms see Fig. 3b). This vector will be used to compare in a single plot the TCs simulation results with the experimental data.

During normal operation, the LBE moves downward in the HX leg, upward in the MH and in the 3D legs. However, during transients, the flow direction in all legs can reverse, depending on heater power and initial conditions.

The secondary loop is a closed system using synthetic organic Dowtherm RP heat transfer fluid to cool the main loop. The fluid flow is clockwise (refer to Fig. 1): from the oil tank, through the rotary pump, to the main loop heat exchanger, then through the secondary heat exchanger (designed to remove up to 40 kW), and back to the oil tank.

For validation of the coupled tools, the transition from forced to natural circulation has been considered to emphasize the importance of feedback mechanisms and the efficacy of the coupling methodology. The transient initiates from a forced steady-state circulation with a mass flow rate of 3.34 kg/s in the HX leg, divided between the MH leg (2.03 kg/s) and the 3D-TS leg (1.31 kg/s). Throughout the transient, both the MH and the 3D-TS heater operate continuously with 3.2 kW and 4.0 kW, respectively. The theoretical principle to exploit the three-dimensional effects of the 3D-TS is based on the opposing effect of entering nozzle jet, which enhances fluid mixing inside the test section, and the buoyant boundary layer on the wall externally heated by the source system, which contributes to the formation of thermal stratification.

In forced steady-state circulation (FC) the jet at the 3D-TS bottom is powerful enough to mix the fluid inside the volume; once the EPM pump is turned off, the mass flow rate in all legs declines leading to the onset of natural circulation (NC), driven by temperature gradients between the hot and cold legs, determining the reduction of the mixing effect of the jet and the formation of thermal stratification within the pool (Grishchenko et al., 2015).

The transient initial and final steady state conditions are reported in

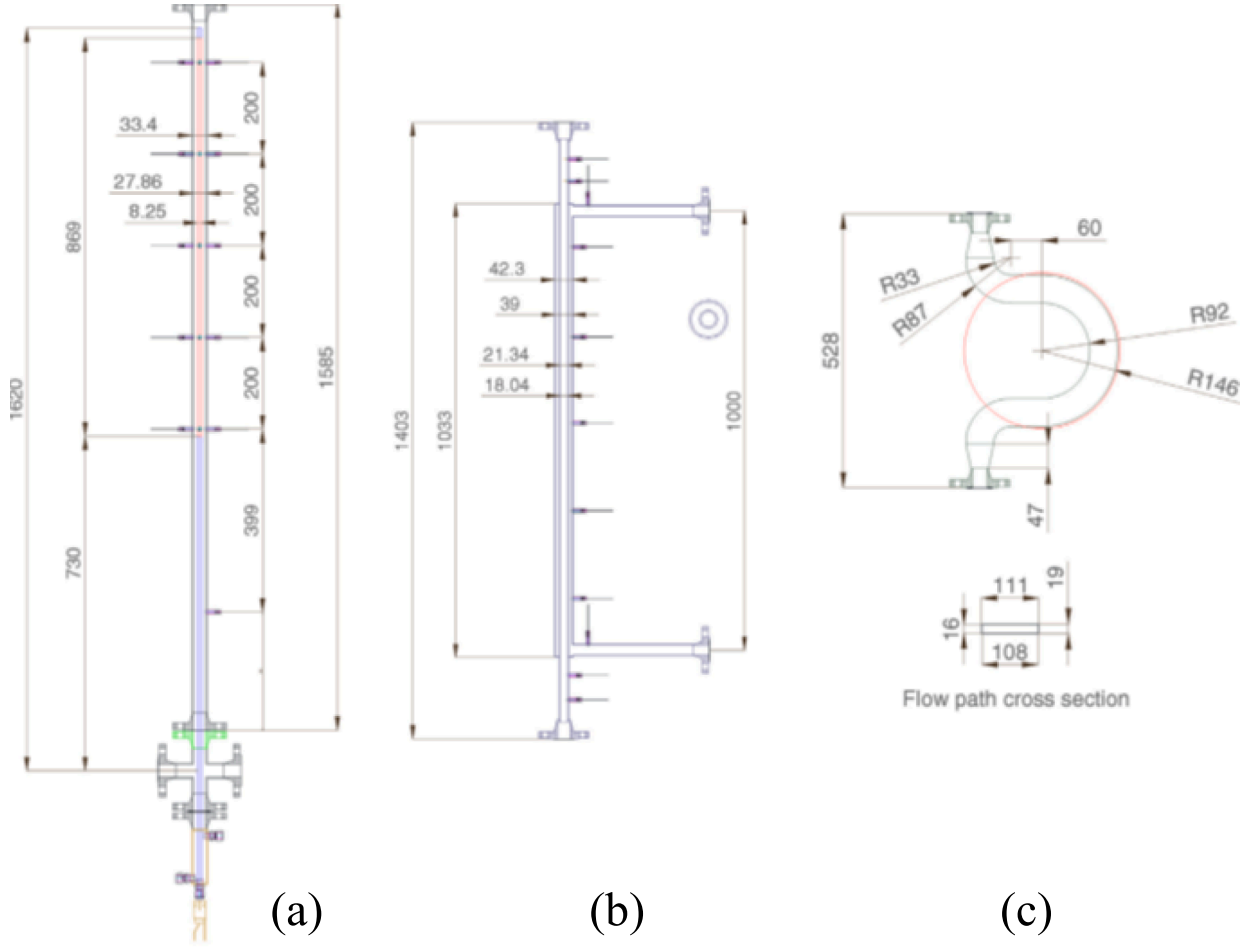

Fig. 2. Design drawings of main loop components (main heater (a); heat exchanger (b); LBE pump (c)) (Grishchenko et al., 2015).

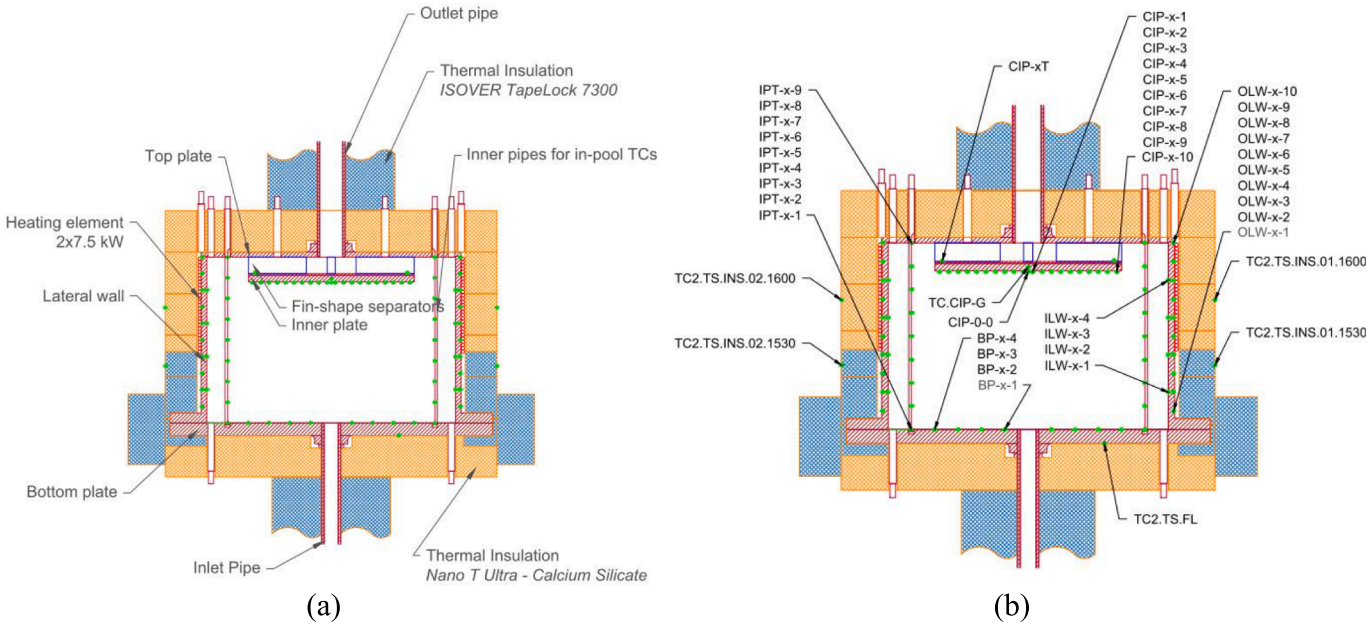

Fig. 3. TALL-3D test section: components (a) and thermocouples position and nomenclature (b) (Grishchenko et al., 2015).

Table 1
Experimental test initial and final steady state conditions.

Parameter	Units	Initial steady state (FC)	Final steady state (NC)
Main heater electric power	W	3234	3235
3D-TS electric power	W	4048	4027
Heat exchanger LBE mass flow rate	kg/s	2.03	0.25
3D-TS LBE mass flow rate	kg/s	1.31	0.27
MH down section LBE temperature	°C	234.5	202.0
MH top section LBE temperature	°C	246.5	283.92
HX top section LBE temperature	°C	250.2	280.0
HX down section LBE temperature	°C	236.0	211.9
3D-TS down section LBE temperature	°C	235.4	201.8
3D-TS top section LBE temperature	°C	254.1	294.7

Table 1 and correspond to the test TG03.S301.04 of the SESAME project (Moreau et al., 2019) first series of test.

3. 3D-test section model

The modelling of the axisymmetric pool in a STH code could be carried with a one-dimensional component featuring an axial discretization along the flow direction. Control volumes with different flow areas can be used to simulate the transition from the loop pipeline to the 3D-TS. In the junctions between volumes that corresponds to a change of area, properly defined localized pressure drops coefficients need to be set up.

The modelling using a CFD code could benefit from the quasi-axisymmetric conditions within the test section. The parts that do not meet the axisymmetric condition are the fin-shaped separators and the thermocouples. However, the impact of the separators can be neglected, and the thermocouples are positioned on four equally spaced planes. To obtain axisymmetric experimental data comparable with simulation results, the average values from the four planes were considered.

An experimental error has been computed as the sum of three contributions:

$$\sigma_{tot} = \sqrt{\sigma_{man}^2 + \sigma_{sym}^2 + \sigma_{std}^2} \quad (1)$$

where:

- σ_{man} correspond to the accuracy indicated by the manufacturer, equal to 1.5 °C;
- σ_{sym} indicates the agreement between the four measuring planes and it is computed as the standard deviation among the four steady state values;
- σ_{std} represent the dispersion, thus the noise of the measures in time and it is computed as the square root of the sum of the square of the four standard deviations in the steady state time interval.

The simulations of the test section model have been carried out with the commercial code Ansys CFX (ANSYS, 2011) with the following set up options:

- the CFD domain includes the fluid, the steel 316L, the heaters (considered made entirely of steel 316L) and the insulation. Materials properties are taken respectively from the handbook of liquid metals for the LBE (OECD/NEA Nuclear Science Committee, 2015), from Ref. Kim (1975) for the steel, and from Ref. Grishchenko et al. (2015) for the insulator;
- at the top (Up) and bottom (Down) section of the domain, two opening boundary condition are imposed, setting the mass flow rate at the bottom section with uniform velocity distribution on the area and relative pressure equal to zero at the top;
- the buoyancy forces are taken into account;
- the power to the test section is provided by mean of a uniform volumetric heat source in the heaters domain;
- the SST k-ω turbulence model (Menter, 1994) is implemented with a constant turbulent Prandtl number equal to 2 (Martelli et al., 2017). Variation of the constant turbulent Prandtl number in the range 1.5–3 have been tested showing negligible differences;
- an upwind advection scheme is selected in the solver. The High Resolution scheme implemented in CFX has been tested, giving similar results with slower convergence. In transient simulations the solver adopt an implicit scheme.

The axisymmetric condition can be exploited in CFX with a 2D or 3D approach; the former foresees the use of a single cell in the azimuthal direction. Simulations have been carried out with both periodic and symmetric conditions on the azimuthal boundaries.

On the 2D model, a grid independence study has been carried out with the condition corresponding to the first steady state of the transient previously described and reported in Table 2.

Even if the global quantities variation is almost unchanged between the three meshes, the temperature in the TCs position is affected by the spatial discretization. Mesh 2 has been selected since the maximum temperature difference with respect to the reference Mesh 1 is lower than the TCs accuracy proposed by the manufacturer.

Mesh setting parameters have been selected equal to the one of Mesh 2 (Fig. 4) and they are adopted also for all the other models on the azimuthal faces.

To follow, the effect of 2D or 3D modelling, and the dimension of the circumferential angle considered in the 3D cases is evaluated by comparing the results with the experimental ones (see Fig. 5 and Fig. 6). Models with 3° and 90° angles have been built with 5 and 150 radial points respectively. In addition, since the symmetry could be addressed not only with the symmetric boundary conditions, but also with the periodic condition, the latter has been tested on the 3° model.

The qualitative fluid temperature trend inside the box is well captured by all the models except for the ILW TCs (i.e., the ones on the internal faces of the box) in the initial steady state, where, in any case, the error is limited. Among the presented cases, negligible differences have been noticed, also on the pressure drops across the test section. For this reason, the 2D model will be adopted for the coupled approach, in order to reduce as much as possible the computational cost.

The error on the fluid temperature measurement in the TCs positions inside the test section is always lower than 10 °C in both the steady states. However, it has been noticed that was not possible to reach a good agreement in the energy balance, since the CFD model seems to underestimate the thermal losses through the insulation: a possible explanation could be the thermal bridges located in the penetration of instrumentation support through the insulation, located on the horizontal surfaces top and bottom of the 3D-TS and mainly on the upper surface. Due to the importance of reproducing the thermal balance inside the test section, for the coupled simulation an *improved* model has been defined with region in the insulation with an increased thermal conductivity, computed as the mean value between the insulation and steel one. In this way, the CFD model is able to reproduce the experimentally measured thermal losses and results in improved TCs temperature representation, especially in the final steady state (see red trends in Fig. 5 and Fig. 6).

In Fig. 7 and Fig. 8, the temperature distributions inside the 3D-TS for the initial and final steady states are reported. Since the provided power from the heaters is the same, the thermal gradients are much higher in the final steady state. It could be clearly noticed in the initial steady state how the inlet jet is able to achieve a good pool mixing, with temperatures at the lower face of the pool close to the exit one. On the contrary, when the final steady state is achieved, the thermal stratification is visible in all the pool except for a limited region over the inlet section.

Table 2
Grid independence study of the 2D model of the 3D Test Section.

Quantities	Mesh 1	Mesh 2	Mesh 3
N° of cells [–]	187.5 k	109.2 k	38.9 k
Temperature up section [°c]	256.1	256.1	256.1
ΔP [Pa]	1001	1011	999
Average temperature error at the TCS with respect mesh 1 [°C]	–	0.15	0.62
Maximum TCs error respect mesh 1 [°C]	–	1.11	6.88

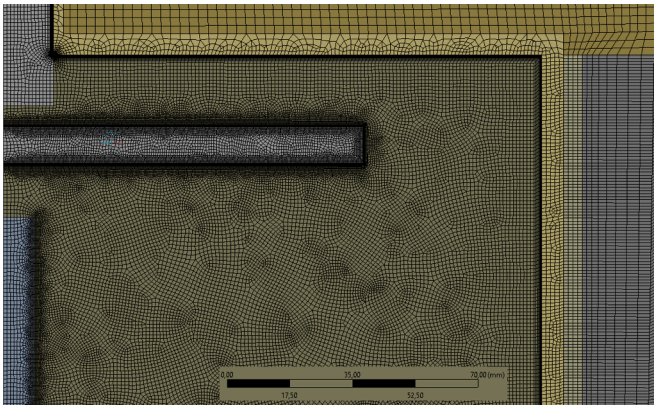

Fig. 4. Detail of the discretization in Mesh 2.

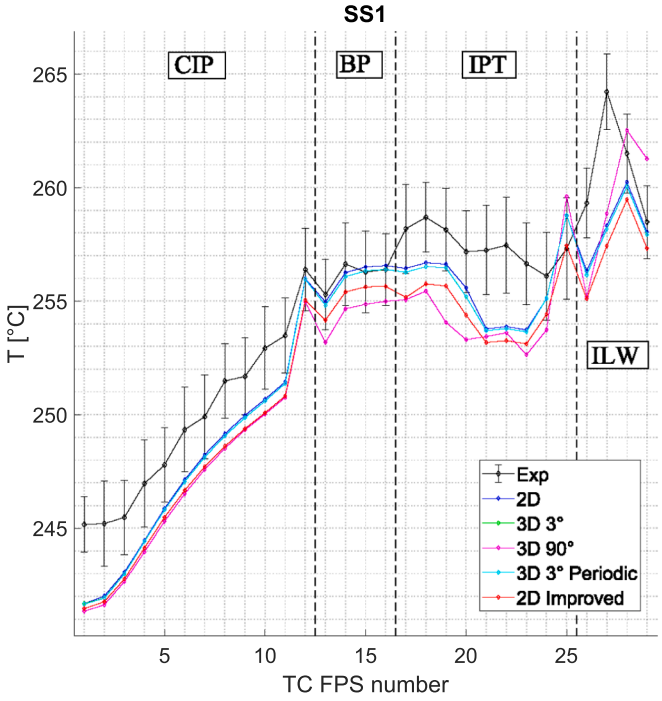

Fig. 5. Comparison with experimental data of the different modelling approaches of the 3D-Test Section during the initial steady state.

After the assessment of the overall behaviour of the CFD model in steady state conditions a transient simulation with experimental boundary conditions has been performed, to give confidence in the application of the CFD-STH coupled tool. Imposing the experimental mass flow rate and inlet/outlet temperatures, the model has been tested evaluating the capability to reproduce the phenomena inside the pool.

In Fig. 9 the temperatures monitored at the lower (Down) and upper (Up) 3D-TS boundaries are reported for the *reference* case without correction on the thermal conductivity of the insulation and the *improved* model defined to match the heat losses (which has already proven to better estimate the temperature field in steady state condition). The zero of the time axes in the transient plots has been set equal to the instant at which the magnetic pump has been shut down. The temperatures are forced by simulation set up to coincide with the experiment at the upper section in the time range where the mass flow rate goes from the top to the bottom (75 s–260 s) and at the lower section otherwise. Looking at the temperatures trends, it could be noticed differences in the prediction of the system thermal dynamic, in particular for what concern the peak reached at the Up boundary during the

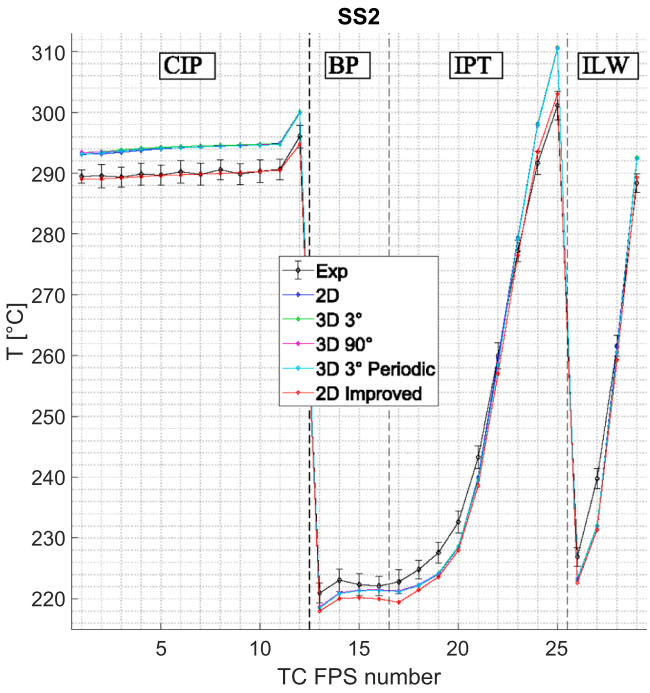

Fig. 6. Comparison with experimental data of the different modelling approaches of the 3D-Test Section during the final steady state.

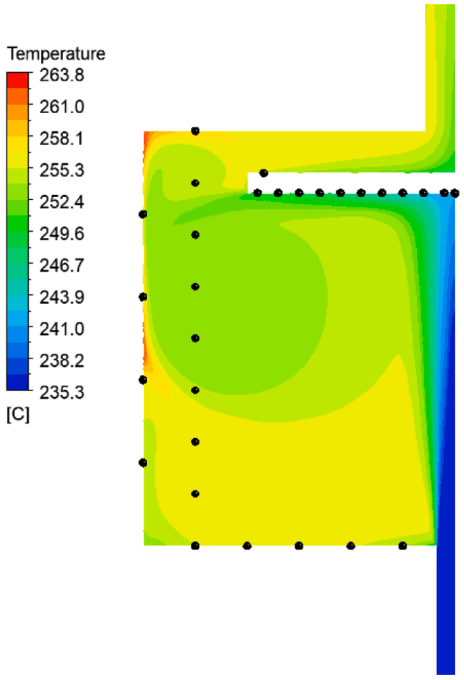

Fig. 7. Temperature distribution inside the 3D-Test Section during the initial steady state with the 2D improved model.

transient: the *reference* case over predicts the maximum value, while the *improved* one slightly under predicted that value but shows very good agreement with experimental data during the remaining part of the transient. The performance achieved with the 2D *improved* CFD model has been considered satisfactory for the coupled application.

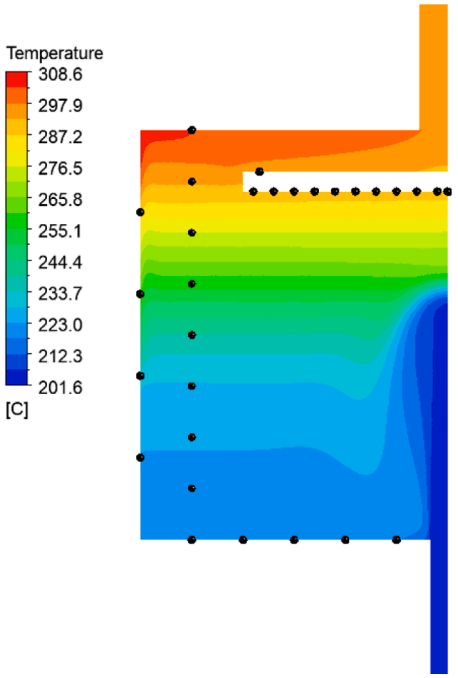

Fig. 8. Temperature distribution inside the 3D-Test Section during the final steady state with the 2D improved model.

4. System scale model

The facility has been simulated through pipes, junctions and pump RELAP5 components (Fig. 10). A total of 380 fluid volumes have been used to discretize the entire volume, each with an average mesh length of 5 cm, maintaining a mesh length-to-diameter ratio greater than 1, and adopting the "sliced modelling approach" (Narcisi et al., 2019); i.e., fluid elements belonging to different regions (e.g., legs) but located at the same quote have been discretized with the same vertical mesh. The primary fluid is LBE, and the free level is set in pipe 134, where the pressure boundary condition is imposed thanks to the time dependent volume 140. It has been possible to realize the interface between LBE and argon thanks to the modification to the source code, allowing the coexistence of Heavy Liquid Metals (HLMs) and a gas phase in the same fluid volume (Oriolo, 2000; Martelli et al., 2019; Forgione, 2019). The electromagnetic pump (in the green box in Fig. 10) has been simulated with the PUMP component, that is intended to be a mechanical pump in RELAP5. Therefore, proper modifications have been done to adjust the power provided to the LBE by the pump. Evaluation of T-junctions pressure loss coefficients has been performed according to Ref. Idelchik (2007), while flow meters and ball valves pressure losses have been calibrated according to Ref. Grishchenko et al. (2015).

Though the secondary fluid is a diathermic oil named Dowtherm RP, water with proper modifications to the operative conditions has been used in the secondary side of the heat exchanger because of the lack of such fluid in RELAP5. Temperature, pressure and mass flow rate boundary conditions are set by time dependent volumes and a time dependent junction.

Heat transfer with the solid structures has been simulated by heat structure components. In particular, the MH and the 3D-TS heating rod/cables have been simulated by structures with internal heat generation, while the heat transfer from LBE to the secondary fluid is modelled through a heat structure with the thickness of the tube. Additional solid structure such as valves and flow meters have been simulated by adiabatic structures to consider the thermal inertia of the metal. Heat losses towards the environment has been considered through an insulator layer, and the environment has been simulated with constant heat transfer coefficient and temperature, respectively equal to 8 W/m^2 K and

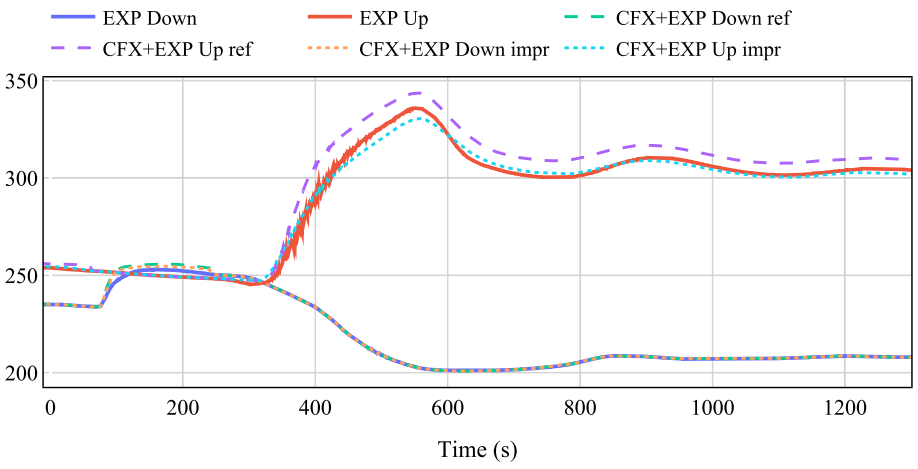

Fig. 9. Transient simulation with the Ansys CFX model and boundary conditions from experimental results.

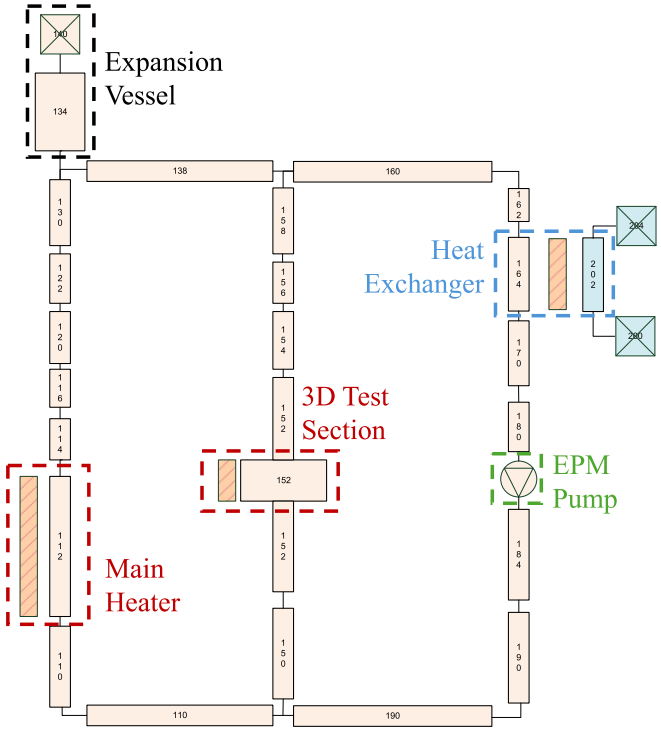

Fig. 10. RELAP5 nodalization of TALL-3D facility.

10 °C.

For the coupled simulation, the modelling of the system is modified accordingly to the procedure foreseen for the selected spatial discretization approach (see Section 5).

5. Coupling tool

The Ansys CFX – RELAP5/Mod3.3 coupled tool adopts a dedicated solver for each code, with a two-way information exchange. The time-step of the STH code can be a submultiple of the CFD one, but the information exchange occurs always at the end of the CFD time-step. The codes run sequentially, exploiting the negligible CPU time taken by the RELAP5 run with respect to the CFD time-step (Pucciarelli, 2020).

Ansys CFX is the master code of the coupling tool and adopts in-house developed FORTRAN subroutines and Python written executables to manage the information exchange, RELAP5 input definition and post processing, and the synchronization between codes.

The code coupling has been implemented in previous works adopting both domain decomposition and overlapping approaches and both the explicit and semi-implicit time advancing schemes, demonstrating the reliability of the different solutions in cases with increasing complexity (Cioli Puviani et al., 2025). The difference between the explicit and semi-implicit time advancing schemes consists in the time location within the simulation flow in which the two codes exchange information and eventual iteration of the coupling time step.

The explicit scheme involves the exchange of information between codes at the end of the CFX time-step: this choice determines a simpler coupling approach, that runs with a lower computational time but in general present numerical instabilities at higher time-step. On the other hand, in the semi-implicit scheme codes communicate within the CFX time-step at the end of each internal iteration, determining a more robust simulation. In this approach, boundary conditions are iteratively adjusted until they meet a user-defined tolerance or the maximum iteration count is reached.

In each internal iteration, RELAP5 runs a simulation for the duration of the coupled time-step using updated and informed boundary conditions. The convergence check is carried out on the CFX's boundary conditions to allow the code to run with a single CFX iteration if the variation of the parameters is negligible. To manage oscillations, a user-defined under-relaxation factor is introduced to moderate the change in boundary conditions between iterations.

In the decomposition domain approach, the entire system is divided into two separate domains, one simulated by the STH code and one by the CFD code. The exchange of information occurs at the boundaries of the domains. With the overlapping approach, the STH code simulate the entire system, including the part simulated by the CFD code, which gives feedback to the STH computing internal code parameters.

The detailed description of the coupled tool and preliminary test cases results could be found in Cioli Puviani et al. (2025).

5.1. An alternative overlapping domain approach

In the previous work (Cioli Puviani et al., 2025), the overlapping domain was based on the continuous correction of a local pressure drop coefficient (K) in a junction of the RELAP5 model with the goal of matching the CFD computed pressure drop. The formulation is here reported:

$$K^{j} = K^{j-1} + s \bullet \frac{\left(\Delta p^{j-1}_{CFX} - \Delta p^{j-1}_{RELAP5}\right) + \left(\Delta p^{j-2}_{CFX} - \Delta p^{j-2}_{RELAP5}\right)}{2} \bullet \Delta t \bullet sign(v_{inlet}) \tag{2}$$

where the terms involved in the correlation are:

- a multiplication user-defined scaling factor (s) to give the possibility to relax the K variation: higher values of scaling factor tend to speed up the convergence of the two pressure drop values. However, if a too large value is selected, it could determine an unstable solution (oscillatory or divergent). This value is not known a priori and the user should select it by practice and experience;
- the time-step (Δt);
- the Δp_{CFX} and Δp_{RELAP5} corresponding to the pressure variation in the two codes;
- the sign of the velocity ($sign(v_{inlet})$), since the relative pressure drops in the domain should invert its sign if reversed flow condition occurs.

In Eq. (2), the j index indicates the time-steps in the explicit scheme or CFX internal iterations if the semi-implicit scheme is adopted.

Such formulation was simple to implement and do not foresee any fast divergent term in cases where the system fluid flow tends to stop or invert its direction. On the other hand, the correction depends on a user-defined scaling factor that should be calibrated for each simulation and in some cases could lead to numerical instabilities. For this reason, an alternative overlapping domain approach has been developed based on the solutions adopted by Huxford et al. (2023) but applied to Ansys CFX and RELAP5 codes.

The approach simplifies the overlapped domain representation reducing the number of volumes needed in RELAP5 to 3 volumes: a single central volume with the same vertical height of the CFD domain and two small horizontal volumes at the upper and lower boundaries. The horizontal volumes have the function of imposing the temperatures computed by the CFD code by means of "fake" heat structures featured by an infinite thermal conductivity and a negligible heat capacity. The horizontal volumes are set in such a way to not introduce any pressure drop. The vertical volume has the goal to reproduce the CFX pressure variation by defining a suitable friction factor (f_{RELAP5}).

The correlation between the f_{RELAP5} and Δp_{CFX} comes from the momentum conservation equation of the two codes:

$$\text{RELAP5}\Big/\text{Mod3.3}\quad \rho\frac{\partial U}{\partial t}+\frac{1}{2}\rho\frac{\partial U^2}{\partial x}=-\frac{\partial p}{\partial x}-\frac{1}{2}\frac{f_{RELAP5}}{D_h}\rho U|U|-\rho g \tag{3}$$

$$\text{Ansys CFX}\quad \rho\frac{\partial \boldsymbol{U}}{\partial t}+\rho \mathrm{U}\bullet\nabla \mathrm{U}=-\nabla p+\rho\nabla\bullet\boldsymbol{\tau}-\rho\boldsymbol{g} \tag{4}$$

In order to match the pressure gradients in Eqs. (3) and (4), the friction term of the RELAP5 equation should be directly correlated with the pressure gradient correcting for the other terms, from left to right: local acceleration, convective acceleration and gravitational terms.

Especially with an explicit coupling scheme, it is not straightforward to correct for the local acceleration term in the STH code, since this term results from velocity updates at each time step. However, since the application of the tool regards incompressible flow, it is reasonable to assume that the difference between the local acceleration as computed by CFX and RELAP5 for the overlapped domain is negligible as long as fluid velocities are consistent. In the coupled tool this is done by ensuring the same flow area and inlet temperature, the latter by mean of the horizontal volumes previously discussed. Therefore, only the convective acceleration and gravitational terms need to be corrected (Grunloh and Manera, 2016).

Since the overall CFD pressure drop must be matched by the RELAP5 calculation, the sum of the pressure gradient and the local acceleration is substituted in Eq. (3), and the RELAP5 friction factor could be computed as:

$$f_{RELAP5}=\frac{2D_h}{\rho U|U|}\left(\left[-\frac{1}{V}\int_V\left(\nabla p+\rho\frac{\partial \boldsymbol{U}}{\partial t}\right)\bullet\hat{n}dV\right]_{CFX}-\frac{\rho}{2}\frac{\partial U^2}{\partial x}-\rho g\right) \tag{5}$$

The scalar product between the CFD terms ("3D" terms) and the versor $\hat{n}$ parallel to the flow direction has been performed to convert them in "1D" elements, making them consistent with the RELAP5 1D formulation of the momentum equation. Therefore, only the projection of such vectors along the RELAP5 flow path has been considered. The CFD informed term ($[\ldots]_{\mathrm{CFD}}$) is evaluated explicitly in the following way:

- $\frac{1}{V}\int_V(\nabla p\bullet\hat{n})dV=\Delta p_{CFX}/L=(p_{outlet}-p_{inlet})/L$. It is the pressure difference across the boundaries divided by their distance, i.e., their difference in absolute height;
- $\frac{1}{V}\int_V\left(\rho\frac{\partial \boldsymbol{U}}{\partial t}\bullet\hat{n}\right)dV=\frac{1}{V}\int_V\rho\frac{\partial U_x}{\partial t}dV$. It is the volume average of the time derivative of the velocity along to the flow direction.

To avoid inconsistencies of results due to differences in the density values between the codes, the temperature corresponding to the volume averaged density in the CFX domain has been imposed in the RELAP5 vertical volume by mean of another "fake" heat structure. The most appropriate density value would be the integral along the vertical flow direction in the domain, but the volume averaged has been considered a good approximation and selected because of its simplicity.

As shown in the following sections, when the velocities approach zero, thus when there is a stagnant flow or a flow inversion, this approach could lead to numerical inaccuracy. The presence of the square of the velocity in the friction factor definition, the importance of gravity term with respect to the other terms (especially true with HLMs) and the approximation of the average density in the CFD domain are possible sources of discrepancies between pressure drop computed from the CFD model and the one obtained in the overlapped domain. This overlapping approach could be difficult to implement if "closed" codes are coupled, in which the accessibility and malleability of the codes are limited. In the future, further implementations could be carried out to improve the approach in conditions where flow inversion is present. An additional improvement related to the STH code could be carried out allowing the user to define the friction factor by mean of RELAP5 "control variables" components: in this way the implicitness of the methodology could be enhanced favouring the robustness of the method even with an explicit approach.

5.2. Comparison between the different coupling approaches

In the TALL-3D simulations, the coupling between the codes consists in the exchange of the following information:

- the CFX code receives the mass flow rate and temperatures at the boundaries;
- the RELAP5 code receives the mass flow rate, temperatures and pressure at the boundaries in the decomposition approach, or the friction factor/pressure loss coefficient and temperatures at the boundaries and of the single vertical volume in the overlapping approach.

The first test of the tool consists in the application of the decomposition approach with both the explicit and semi-implicit time advancing schemes at different coupling time-steps. The results of the mass flow rate in the 3D-TS leg are reported in Fig. 11. The legend of the figures indicates the method ('ex', explicit or 'si', semi-implicit) and the time-step between two exchanges of information that coincides with the CFX time-step. The RELAP5 time-step has been kept constant and equal to $2{\cdot}10^{-2}$ s.

The explicit scheme shows numerical oscillations with a high time-step (5e-1s) as soon as the transient starts, but it is possible to define a time step at which the oscillations disappear. No oscillations have been noticed when the semi-implicit scheme is adopted. The numerical oscillations, if present, are dumped after a short period of time. After, the results are practically equals to the ones without oscillations.

Employing both time advancing schemes, the major discrepancies

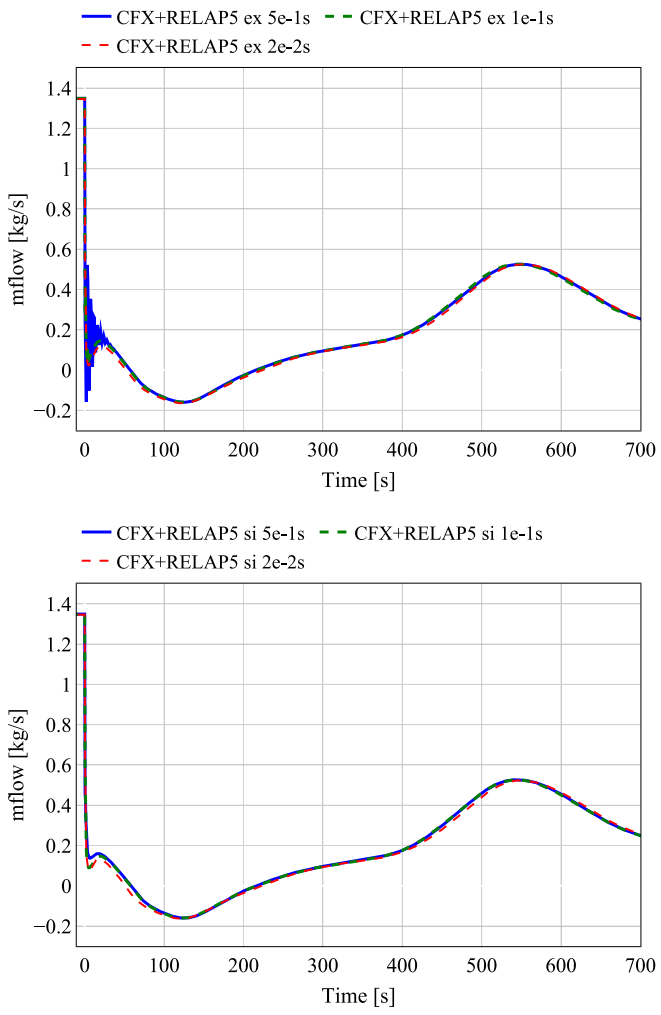

Fig. 11. Coupled simulation with the decomposition domain approach at different coupling time-step with the explicit (top) and semi-implicit (bottom) time advancing schemes.

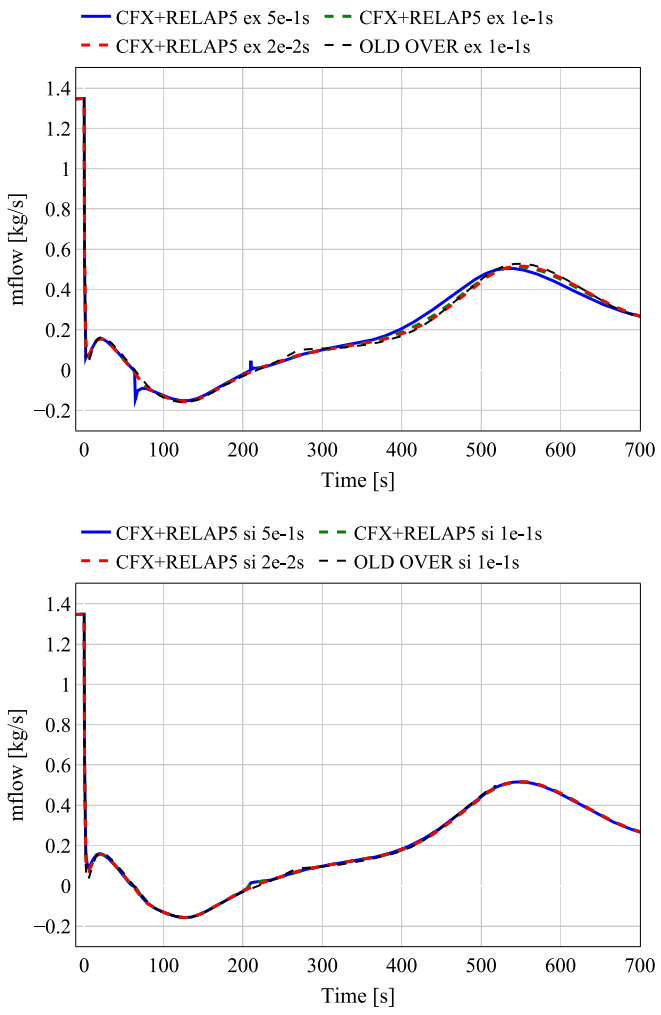

Fig. 12. Coupled simulation with the overlapping domain approach at different coupling time-step with the explicit (top) and semi-implicit (bottom) time advancing scheme.

could be noticed during the fast reduction of mass flow rate due to the magnetic pump stop: lower time-steps tend to show lower values in the first minimum. Nevertheless, the results almost coincide after around 100 s and there are no notable differences between explicit and semi-implicit schemes.

In Table 3, a comparison of the computational time required by the different simulations at various time-steps and with both the time advancing schemes are reported. The comparison has been carried out with the same solver set up and the same computational power (24 CPU). The time required from the semi-implicit scheme is around 1.5 times larger than the explicit one.

The same calculations have been repeated with the overlapping approach for both the explicit and semi-implicit time advancing schemes (Fig. 12), along with a comparison with the results obtained adopting the overlapping approach presented in Cioli Puviani et al. (2025) (OLD OVER in the legend of Fig. 12), based on the continuous correction of the junction pressure loss coefficient. Also in this case, the dependency on the time step is limited except for the explicit scheme at the highest time-step, where some mass flow rate numerical distortions are visible as soon as the velocity approach the zero and inverts its sign, determining local spikes because of numerical discontinuities in the friction factor calculation. No oscillations are present in the overlapping simulations.

The differences with respect to the old version of the overlapping approach are minimum demonstrating the validity of both formulations.

The computational time needed for the simulations with the overlapping approach has negligible differences with respect to the decomposition one, reported in Table 3, and thus not showed in this work.

Eventually, Fig. 13 shows the overlay of the results obtained with a time-step of 1e-1 s for both explicit and semi-implicit time advancing schemes, implementing the decomposition and both overlapping domain approaches. The plot shows that the variance of the solution is limited, demonstrating the independency of the results with respect to the selected coupling approach.

Table 3
Computational time with the decomposition domain approach at different time-step for the explicit and semi-implicit time advancing schemes.

Coupling time-step	Explicit	Semi-implicit	Semi-implicit/explicit ratio
2e−2 [s]	5.399e5 [s]	7.618e5 [s]	1.41
1e−1 [s]	1.336e5 [s]	2.186e5 [s]	1.64
5e−1 [s]	4.092e4 [s]	6.461e4 [s]	1.58

5.3. *Validation against experimental results*

The comparison of the coupled tool with experimental data and the RELAP5/Mod3.3 standalone simulation shows a clear advantage of the CFD code in representing the phenomena occurring in the test section and their effect on the facility behaviour. The simulations with the decomposition approach, the semi-implicit time advancing scheme and

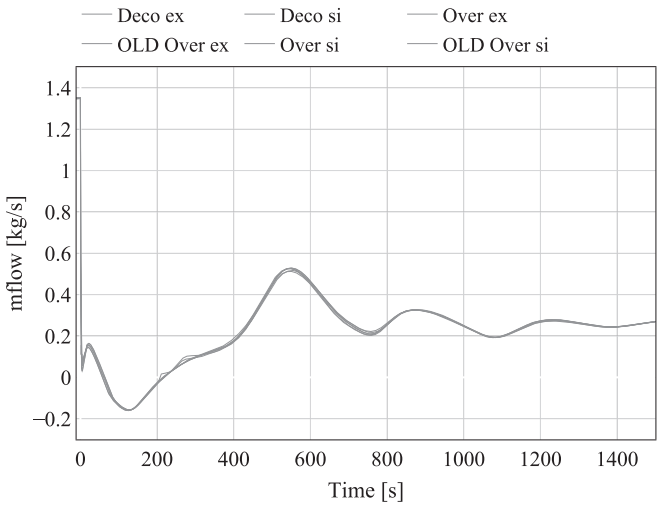

Fig. 13. Overlay of the mass flow rate in the 3D test section leg for all presented coupling approaches with a time-step of 1e-1s.

a time-step of 1e-1 s have been selected as reference coupled simulation. In Fig. 14, the coupled simulation with the decomposition approach shows improvements in reproducing the frequency of the experimental oscillations of the mass flow rate in the 3D-TS, even though their amplitude is slightly higher than the numerical ones. Similar conclusions could be drawn analysing the mass flow rate on the MH leg (Fig. 15), with a notable improvement in the phenomena representation by the coupled approach.

The reason behind this behaviour could be found especially in the temperature at the 3D-TS model boundaries (Fig. 16):

- the temperature at the lower section predicted by the CFX-RELAP5 tool is perfectly reproduced in the first rise, the latter determined by the inversion of the mass flow rate, demonstrating a good representation of the initial steady state inside the test section and the prediction of flow reversal. However, the trend is under-predicted by both the coupled and standalone simulations for the remaining part of the transient, probably because of the use of a different secondary fluid in the HX instead of the synthetic organic Dowtherm RP fluid, causing different performances of the component;
- the temperature at the upper section is slightly under-predicted at the peak due to the higher thermal capacity of the CFD model demonstrated in Fig. 9 and because of the lower temperature at the Down section, but an improvement in the representation of the oscillation frequency is visible;
- at the final steady state, the temperature variation across the 3D-TS is slightly lower in the experiments because of a slightly higher mass flow rate.

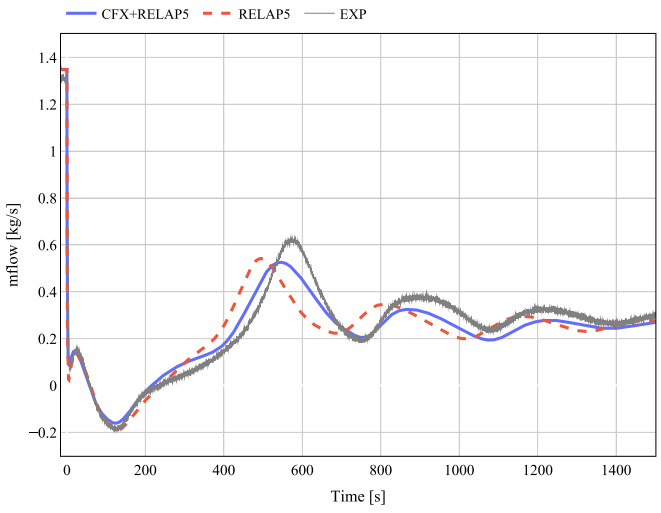

Fig. 14. Comparison between experiment, RELAP5 standalone and coupled simulation of the mass flow rate in the 3D test section leg.

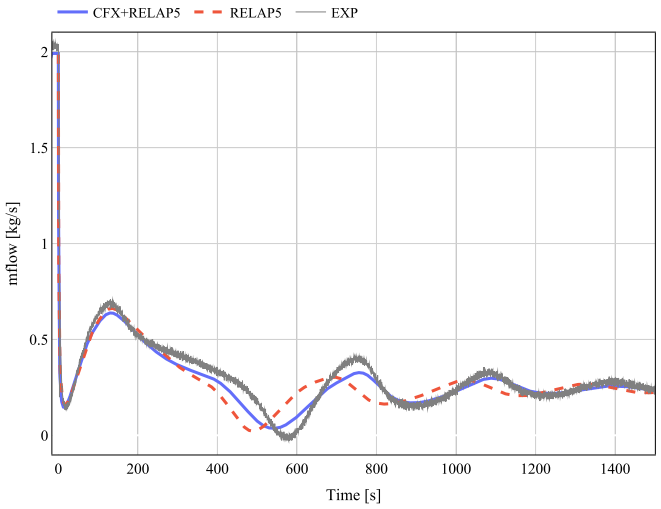

Fig. 15. Comparison between experiment, RELAP5 standalone and coupled simulation of the mass flow rate in the Main Heater leg.

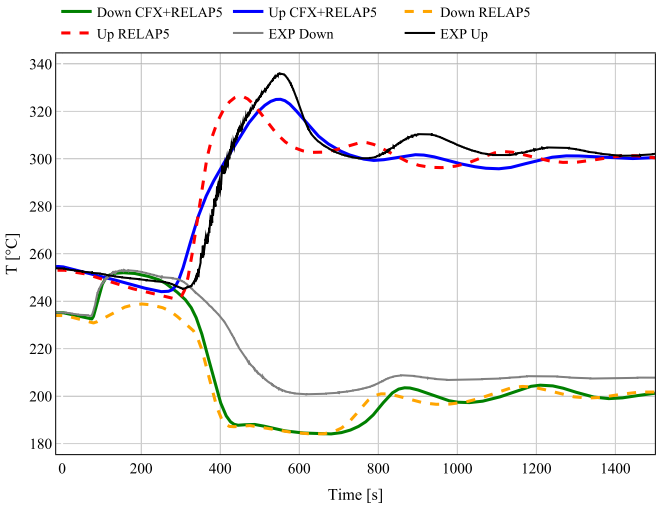

Fig. 16. Comparison between experiment, RELAP5 standalone and coupled simulation of the upper and lower surface temperature of the 3D test section.

The Ansys CFX – RELAP5/Mod3.3 tool gives the possibility to compare the results of the TCs inside the pool also during the transient. The IPT and CIP TCs have been selected for this purpose. The IPT TCs are mounted on the vertical support, covering the entire length of the pool, while the CIP TCs are positioned on the horizontal plate. (Fig. 3a). The results of the decomposition approach simulation (CFX + RELAP5, dashed lines) in Fig. 17 show a good agreement in the upper region of the pool (IPT 1–3) located closer to the heaters. Going down in the pool the IPT temperatures are under-predicted: the reason could be found in a local bad prediction of the thermal losses, that gain more importance when the mass flow rate is reduced, or a slightly worse performance of the CFD model in the transition toward an almost fully conductive heat transfer condition within the fluid, or behind the underestimation of the temperature entering the pool from the lower section. In Fig. 17 the

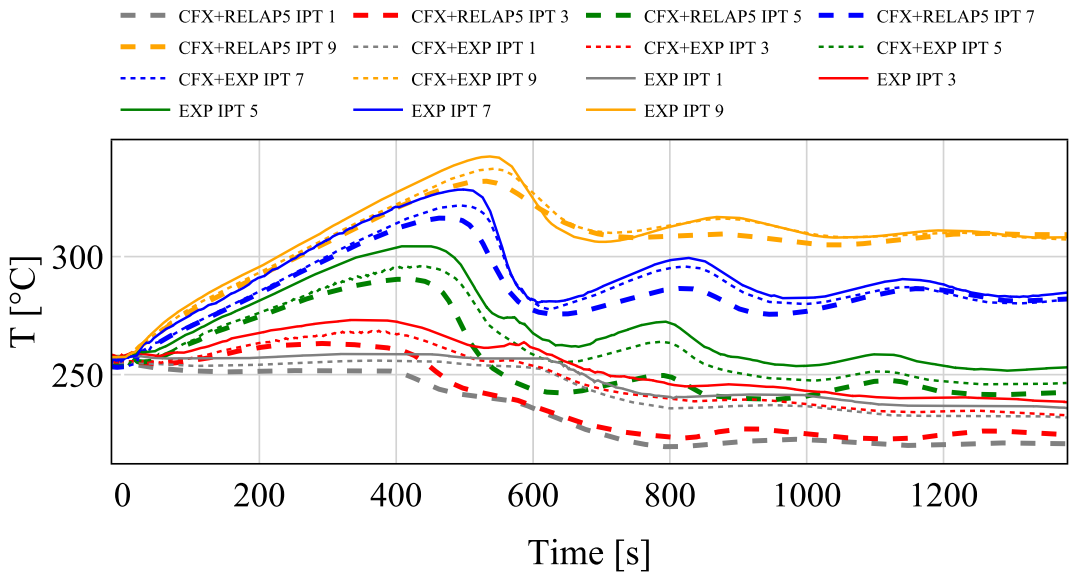

Fig. 17. Comparison between experiment, coupled decomposition simulation and CFX transient simulation of IPT thermocouples inside the 3D test section.

dotted lines represent the results obtained with the CFX model in which the experimental boundary conditions are applied (CFX + EXP), already discussed in Section 3 (*improved* model). The results are closer than the coupled simulation ones to the experimental values, considering also the IPT TCs located in the lower part of the pool. This fact supports the idea that the errors are related to the underestimation of the temperature entering the pool from the lower section.

In Fig. 18, the CIP temperatures could be described as follows:

- in the first 450 s the CFX + EXP and CFX + RELAP5 results under-predict the experimental value;
- from 630 s toward the final steady state of the CFX + RELAP5 calculation, results are under-predicted, with a similar behaviour seen in the IPTs and lower section temperatures;
- between 450 s and 630 s, the experimental results show a drop of temperature due to the injection of cold fluid in the pool. This is captured only for the central TCs in the horizontal plate (e.g. CIP 1) by the CFX + EXP simulations, while this trend is not reproduced by the others (e.g. CIP 5 and 10). In the CFX + RELAP5 simulations the drop of temperature is not predicted for any TCs, mainly due to the differences in the mass flow rate and the temperature at the lower section.

6. Conclusions

The Ansys CFX – RELAP5/Mod3.3 coupled tool developed by ENEA has been tested by simulating a forced to natural circulation transition in the LBE-cooled TALL-3D facility. The tool allows the simulation of the 3D test section by the CFD, which demonstrated to be a reliable tool in reproducing steady state temperature distribution in both forced circulation – when the mixing in the pool is notable – and in natural circulation, where thermal stratification occurs.

The effect of the adoption of explicit and semi-implicit time advancing schemes has been exploited, showing numerical instabilities in the explicit scheme at the highest time-step, whereas the result dependency on the time-step is almost absent, especially, far away from the beginning of the transient.

An alternative overlapping approach has been implemented and tested together with the previously presented overlapping method and the decomposition approach. The variance of the results is limited

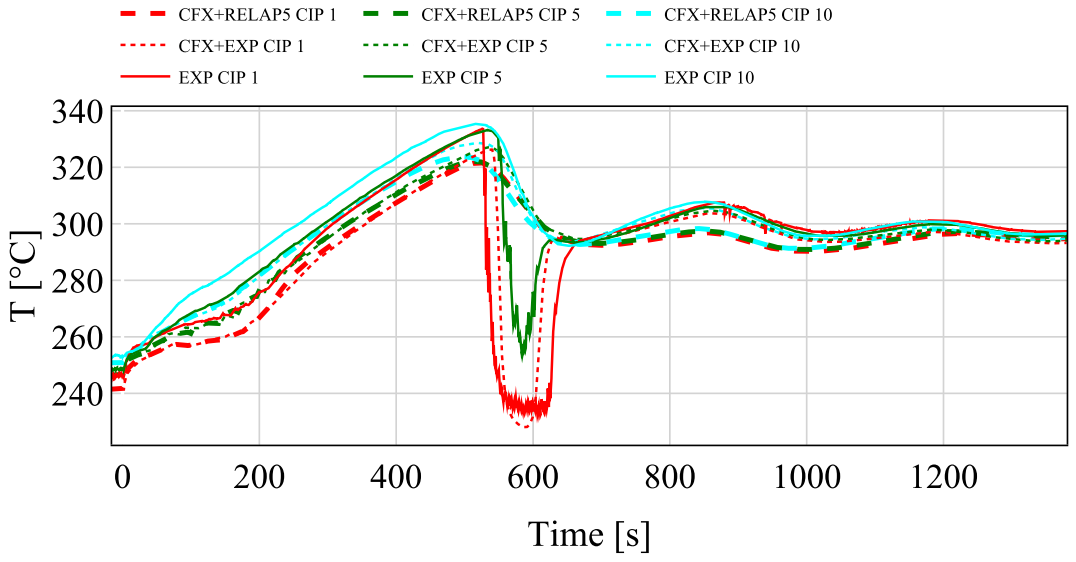

Fig. 18. Comparison between experiment, coupled decomposition simulation and CFX transient simulation of CIP thermocouples inside the 3D test section.

demonstrating the validity of both methods for the considered test case and that the different limitations could be overcome by a proper user selection of the set up parameters. The limitations of each method are:

- decomposition approach: numerical oscillation at high time-steps with an explicit time advancing scheme;
- overlapping approach based on the junction pressure loss coefficient: possible dependence of the results on the selected scaling factor, which could introduce numerical oscillations;
- overlapping approach based on the friction factor: problems when the velocity tends to zero due to the divergence of the friction parameter.

The overall comparison between the coupled tool results and the experimental results demonstrates improvements in the phenomena representation with respect to the RELAP5/Mod3.3 stand-alone model. In particular, the coupled tool is able to reproduce the frequency of the mass flow rate oscillations in the 3D-TS with good accuracy, while maintaining the capability to predict their amplitude. The improvement could be noticed also on the temperature, being the coupled tool able to capture also the initial peak at the 3D-TS lower boundary due to the inversion of the mass flow rate. A further advantage of the coupled tool with respect to the STH-only simulation consists in the local insight within the 3D-TS, giving the possibility to understand in detail the complex multidimensional phenomena occurring within the component.

CRediT authorship contribution statement

P. Cioli Puviani: Writing – original draft, Investigation, Conceptualization. **T. Del Moro:** Writing – original draft, Methodology, Conceptualization. **B. Gonfiotti:** Writing – review & editing, Software, Methodology. **D. Martelli:** Writing – review & editing, Methodology. **C. Ciurluini:** Writing – review & editing, Supervision. **F. Giannetti:** Supervision, Conceptualization. **R. Zanino:** Supervision. **M. Tarantino:** Supervision, Resources.

Declaration of competing interest

The authors declare that they have no known competing financial interests or personal relationships that could have appeared to influence the work reported in this paper.

Data availability

The data that has been used is confidential.

References

ANSYS, 2011. ANSYS CFX-Solver Theory Guide.

Bandini, G., Polidori, M., Gerschenfeld, A., Pialla, D., Li, S., Ma, W.M., Kudinov, P., Jeltsov, M., Kööp, K., Huber, K., Cheng, X., Bruzzese, C., Class, A.G., Prill, D.P., Papukchiev, A., Geffray, C., Macian-Juan, R., Maas, L., 2015. Assessment of systems codes and their coupling with CFD codes in thermal–hydraulic applications to innovative reactors. Nucl. Eng. Des. 281, 22–38. https://doi.org/10.1016/j.nucengdes.2014.11.003.

Bertolotto, D., Manera, A., Frey, S., Prasser, H.M., Chawla, R., 2009. Single-phase mixing studies by means of a directly coupled CFD/system-code tool. Ann. Nucl. Energy 36 (3), 310–316. https://doi.org/10.1016/j.anucene.2008.11.027.

Cioli Puviani, P., Del Moro, T., Gonfiotti, B., Martelli, D., Giannetti, F., Zanino, R., Tarantino, M., 2025. A novel Ansys CFX – RELAP5 coupling tool for the transient thermal-hydraulic analysis of liquid metal systems. Prog. Nucl. Energy 180, 105590. ISSN 0149-1970. https://doi.org/10.1016/j.pnucene.2024.105590.

Del Moro, T., Cioli Puviani, P., Gonfiotti, B., Di Piazza, I., Martelli, D., Ciurluini, C., Giannetti, F., Zanino, R., Tarantino, M., 2024. Analysis of the experimental tests performed at NACIE-UP facility through a novel CFX-RELAP5 codes coupling. Nucl. Eng. Design 429, 113676. https://doi.org/10.1016/j.nucengdes.2024.113676. ISSN 0029-5493.

Forgione, N., et al., 2019. Post-test simulation for the NACIE-UP benchmark by STH codes. Nucl. Eng. Des. 353, 110279. https://doi.org/10.1016/j.nucengdes.2019.110279.

Frignani, M., Alemberti, A., Tarantino, M., 2019. ALFRED: A revised concept to improve pool-related thermal-hydraulics. Nucl. Eng. Des. 355, 110359. https://doi.org/10.1016/j.nucengdes.2019.110359.

Gibeling, H., Mahaffy, J., 2002. Benchmarking simulations with CFD to 1D coupling. Technical Meeting on Use of Computational Fluid Dynamics (CFD) Codes for Safety Analysis of Reactor Systems Including Containment. Pisa, Italy.

Grishchenko, D., Mickus, I., Kööp, K., Jeltsov, M., Karbojian, A., 2015. TALL-3D experimental setup description for the first test series. SESAME Project, Deliverable N° D4.3.1_M09.

Grishchenko, D., Jeltsov, M., Kööp, K., Karbojian, A., Villanueva, W., Kudinov, P., 2015. The TALL-3D facility design and commissioning tests for validation of coupled STH and CFD codes. Nucl. Eng. Des. 290, 144–153. https://doi.org/10.1016/j.nucengdes.2014.11.045.

Grunloh, T.P., Manera, A., 2016. A novel domain overlapping strategy for the multiscale coupling of CFD with 1D system codes with applications to transient flows. Ann. Nucl. Energy 90, 422–432. https://doi.org/10.1016/j.anucene.2015.12.027.

Huxford, A., Coppo Leite, V., Merzari, E., Zou, L., Petrov, V., Manera, A., 2023. A hybrid domain overlapping method for coupling system thermal hydraulics and CFD codes. Ann. Nucl. Energy 189, 109842. https://doi.org/10.1016/j.anucene.2023.109842.

Idelchik, I.E., 2007. Handbook of Hydraulic Resistance, English ed. Begell House.

Kim, C.S., 1975. Thermophysical properties of stainless steels (ANL-75-55).

Lorusso, P., Bassini, S., Del Nevo, A., Di Piazza, I., Giannetti, F., Tarantino, M., Utili, M., 2018. GEN-IV LFR development: status & perspectives. Prog. Nucl. Energy 105. https://doi.org/10.1016/j.pnucene.2018.02.005.

Martelli, D., Forgione, N., Barone, G., Del Nevo, A., Di Piazza, I., Tarantino, M., 2014. Coupled simulations of natural and forced circulation tests in NACIE facility using RELAP5 and ANSYS fluent codes. Proceedings of the 22nd International Conference on Nuclear Engineering (ICONE22), Prague, Czech Republic.

Martelli, E., Giannetti, F., Ciurluini, C., Caruso, G., 2019. Thermal hydraulic modeling and analyses of the water-cooled EU DEMO using RELAP5 system code. Fusion Eng. Des. https://doi.org/10.1016/j.fusengdes.2019.02.021.

Martelli, D., Marinari, R., Barone, G., Di Piazza, I., Tarantino, M., 2017. CFD thermo-hydraulic analysis of the CIRCE fuel bundle. Ann. Nucl. Energy 103. https://doi.org/10.1016/j.anucene.2017.01.031.

Menter, F.R., 1994. Two-equation eddy-viscosity turbulence models for engineering applications. AIAA J. 32 (8), 1598–1605.

Moreau, V., Profir, M., Alemberti, A., Frignani, M., Merli, F., Belka, M., Frybort, O., Melichar, T., Tarantino, M., Franke, S., Eckert, S., Class, A., Yanez, J., Grishchenko, D., Jeltsov, M., Kudinov, P., Roelofs, F., Zwijsen, K., Visser, D.C., Badillo, A., Niceno, B., Martelli, D., 2019. Pool CFD modelling: lessons from the SESAME project. Nucl. Eng. Des. 355, 110343. https://doi.org/10.1016/j.nucengdes.2019.110343.

Narcisi, V., Giannetti, F., Caruso, G., 2019. Investigation on RELAP5-3D© capabilities to predict thermal stratification in liquid metal pool-type systems and comparison with experimental data. Nucl. Eng. Des. 352. https://doi.org/10.1016/j.nucengdes.2019.110152.

OECD/NEA Nuclear Science Committee, 2015. Handbook on lead-bismuth eutectic alloy and lead properties, materials compatibility, thermal-hydraulics and technologies.

Oriolo, F., et al., 2000. Modifiche del codice RELAP5 versione MOD3.2 per la simulazione di sistemi refrigerati con leghe di Pb o Pb-Bi. University of Pisa.

Papukchiev, A., Jeltsov, M., Kööp, K., Kudinov, P., Lerchl, G., 2015. Comparison of different coupling CFD–STH approaches for pre-test analysis of a TALL-3 experiment. Nucl. Eng. Des. 290, 135–143. https://doi.org/10.1016/j.nucengdes.2014.11.008.

Pucciarelli, A., 2020. Coupled system thermal hydraulics/CFD models: general guidelines and applications to heavy liquid metals. Ann. Nucl. Energy. https://doi.org/10.1016/j.anucene.2020.107990.

Toti, A., 2018. Development and Validation of a System Thermal-Hydraulic/CFD Codes Coupling Methodology for Multi-Scale Transient Simulations of Pool-Type Reactors. Ghent University (Ph.D. thesis).